Journal of Materials Chemistry

Cite this: J. Mater. Chem., 2011, 21, 11288

www.rsc.org/materials

PAPER

Organic–inorganic nanocomposite bilayers with triple shape memory effect

C. Y. Bae,[a] J. H. Park,[a] E. Y. Kim,[a] Y. S. Kang[b] and B. K. Kim*[a]

Received 17th February 2011, Accepted 9th May 2011
DOI: 10.1039/c1jm10722d

Various amounts of silica nanoparticles were chemically incorporated into amorphous polyurethanes (PU) of two different molecular weights by sol–gel reactions, and the effects were studied in terms of mechanical, dynamic mechanical, dual, and triple shape memory effects (DSME and TSME) of the nanocomposite films. It was found that the silica particles act as multifunctional cross-links as well as reinforcing fillers and significantly augmented the glassy and rubbery state moduli, yield strength, break strength, glass transition temperature, and dual shape memory properties. A cohesive bilayer of the two films fabricated from an interpenetrating polymer network (IPN) exhibited synergistic mechanical properties in the glassy and rubbery states along with two undisturbed glass transitions by which an intermediate plateau region and TSME were demonstrated.

1. Introduction

Shape memory polymers (SMPs) respond to external stimuli, typically heat, and their applications are steadily expanding in areas like smart coatings, adhesives, sportswear, textiles, as well as in packaging materials. Furthermore, ample potential applications have opened in new areas, like for biomedical devices and space materials, with the enhancement of the mechanical performance and multiple functionalizations of SPMs.[1,2] Excellent reviews have been given to such materials due to such recent developments.[3–6]

Very recently, a comprehensive review regarding SMP composites became available.[1] Mechanical reinforcement and functionalization are largely achieved by the physical and chemical hybridization of SMPs with fillers in the form of particles, fibers, platelets or tubes. SMPs can be remotely triggered by an electrical or magnetic field with the addition of a conductive or magnetic filler.[7] Generally, chemical incorporation on the nano-scale is superior to physical blending on the macro-scale due to the fine dispersion achieved and the improved interface between the SMP and the filler. However, the results suggest only partial success.

The chemical incorporation of crystalline polyhedral oligomeric silsesquinoxane (POSS) nanoparticles as the hard segments in shape memory polyurethane (SMPU) resulted in over 99% shape fixity but poor shape recovery (71%) for the first cycle.[8] The physical and chemical incorporation of layered nanoclays augmented the mechanical strength of the SMPU but decreased the shape recovery.[9–11] On the other hand, silica nanoparticles, which are chemically incorporated into the amorphous SMPU as multifunctional cross-links, yielded over 99% shape fixity and shape recovery with minimum cyclic hysteresis in some samples.[12,13]

The triple shape memory effect (TSME) rather than the conventional dual shape memory effect (DSME) has received attention.[14–16] With TSME, the shape changes are not limited to one direction and could offer unique opportunities in medical devices or fasteners. TSME materials should have two separated domains with different transition temperatures, like two-way SMPs which operate reversibly by heating and cooling.[17,18] At the intermediate temperature, high transition domains act as physical cross-links and induce an intermediate plateau region. This, along with the totally glassy and rubbery states of the materials, allows two step shape fixing and shape recovery. Typically, multi-block copolymers, such as segmented PU and PU acrylates, are used due to their ample freedom of property design,[19,20] though the performance design is often limited as compared with the dual SMP. Alternatively, bilayers or multilayers composed of independently designed films could open simple and broad ways to achieve multiple SMPs. Bilayer polymers that consist of two epoxy dual-shape memory polymers have been introduced for TSME.[21]

We chemically incorporated a wide range of nano-structured silica particles (1–5 wt%) into a chain of amorphous PU which allowed ample freedom to control the glass transition temperature (T_g). The PU was end capped with 3-aminopropyltriethoxysilane (APTES) and it was sol–gel reacted with silica particles. The silica particles thus became the multifunctional cross-links for PU where the molecular weight of the PU (Called M_{PU}) becomes the molecular weight between the cross-links (M_C). The cross-link density and elasticity of the materials were easily controlled by varying the M_{PU} and cross-link functionality in a broad range. The triple, as well as dual, shape memory effect was studied with a cohesive bilayer that was

[a]Department of Polymer Science and Engineering, Pusan National University, Busan, 609-735, Korea
[b]Department of Chemistry, Sogang University, Seoul, 121-742, Korea

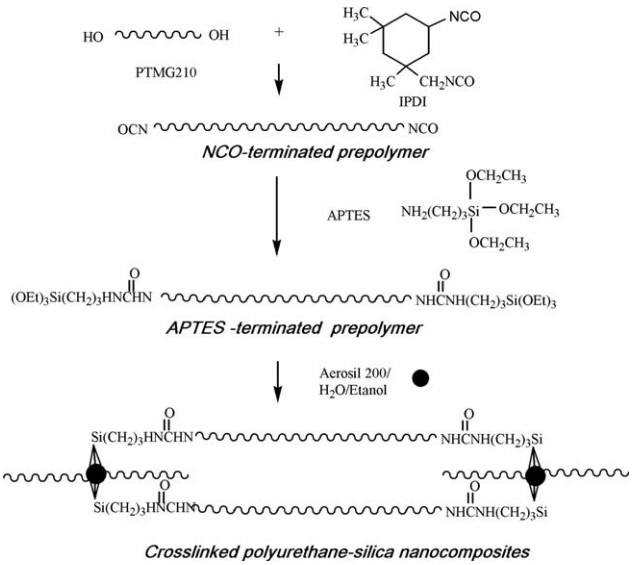

Scheme 1

formed from two films with significantly different T_g values and it was formed according to the interpenetrating polymer network (IPN) technique.

2. Experimental

2.1 Raw materials

Poly(tetramethylene glycol) (PTMG; 210 M_n, KPX, Korea) was dried and degassed at 80 °C under vacuum for 3 h. Isophorone diisocyanate (IPDI, Aldrich), dididbutyltin dilaurate (DBTDL, Aldrich), and APTES (Aldrich) were used as received. Hydrophilic silica (fumed silica, Aerosil 200) with an average primary size of 12 nm, an aggregate size of about 100 nm, bulk density of 3×10^{-2} g cm^{-3}, and 2.5[OH] nm^{-2} was obtained from Degussa.

2.2 Preparation of polyurethane nanocomposites

The overall reaction scheme for the synthesis of the composite is shown in Scheme 1. PTMG was first reacted with IPDI in dimethylformamide (DMF) at 60 °C for 4 h using a 4-necked separable flask equipped with a mechanical stirrer, a thermometer, a condenser, and a nitrogen injection tube. This reaction yielded NCO-terminated prepolymers with theoretical molecular weights of 3000 and 7000 (M_p), that were determined by the index of [NCO]/[OH] > 1. The prepolymer was end-capped with APTES at 60 °C for 3 h. Finally, the various compositions of silica particles dispersed in DMF were fed into the solutions, as given in Table 1. The first digit in the notation indicates the M_p and the second indicates the weight % of the silica. For example, P31 designates a sample with an M_p of 3000 and a silica content of 1 wt%. Based on the formulation and particle characteristics, the following can be calculated.

Total number of particle, $A = 0.74 \times W_s/(\rho_b \times V_p)$, where 0.74 is the maximum packing fraction, W_s = weight of silica, ρ_b = bulk density, and V_p = volume of a particle.

Number of OH groups per particle, $B = S_p \times$ (OH groups/surface area), where S_p = surface area of a particle.

Total number of chain segments, $C = 0.5 \times N_A \times$ mole of APTES, where N_A = Avogadro number.

Number of polymer chain segments per particle, C/A = 736 (1%)–147 (5%). This number is compared with B (283). Since one chain segment has two APTES termini, the OH groups of APTES are in excess which leads to condensation among them.

To improve the dispersion of the silica particles in DMF, the mixture was ultrasonicated for 60 min before it was added to the prepolymer solution. To hydrolyze the ethoxy groups of APTES, a 1 : 1 mixture of distilled water and ethanol (0.2%) were added to the prepolymer solution. Subsequently, the polymer solutions were cast on a Teflon plate and dried to form films. The condensation reactions between the silanol groups of APTES and of the silica surface occurred during the drying in an oven at 80 °C to form cross-links between the PU and silica particles.

A bilayer film was fabricated using the cured P70 and P35 films. To fabricate the film, a minimum amount of the as-synthesized P35 solution was evenly spread between the two cured films and dried at 80 °C for 2 days. The film obtained in this way exhibited excellent interfacial adhesion due to the formation of an IPN structure.

2.3 Measurements

The end capping of the NCO termini with APTES and the sol–gel reactions between the APTES and the Si–OH groups of the silica surface were confirmed by Fourier transform infrared (FTIR) spectroscopy. ^{29}Si cross-polarization magnetic-angle-spinning (CP/MAS) NMR spectra were also recorded using a 7 mm rotor on a Bruker Avance 300.

The tensile properties of the cast films were measured at 25 °C and five runs were made to report the average with a universal testing machine (UTM, Lloyd LRX) at a crosshead speed of 500 mm/min. Detailed data with statistics are shown in Table 1.

Table 1 Formulations to synthesize polyurethane–silica nanocomposites (number is the weight in grams, total solid = 30 g)

						Tensile Properties			
	PTMG210	IPDI	APTES	Silica [%]	M_{PU} [g mol^{-1}]	Initial Modulus [MPa]	Yield Strength [MPa]	Break Strength [MPa]	Break strain [%]
P30	11.34	14.23	4.43	0	3000	607.4 ± 30.5	36.5 ± 3.2	58.70 ± 5.1	168.57 ± 18.5
P31				1		690.34 ± 25.7	40.61 ± 3.1	64.30 ± 4.5	164.28 ± 16.4
P33				3		716.72 ± 27.7	42.3 ± 2.6	64.16 ± 4.8	128.57 ± 15.5
P35				5		812.29 ± 26.5	46.41 ± 3.1	63.27 ± 5.2	107.57 ± 16.8
P70	13.19	14.91	1.90	0	7000	358.72 ± 32.8	29.83 ± 4.2	49.15 ± 6.31	218.57 ± 20.5

Dynamic mechanical tests were performed using a dynamic mechanical thermal analyzer (DMTA) (Rheometrics, MK-IV) at 10 Hz, 5 °C min^{-1}, and 2% strain from −20 to 150 °C.

The morphology of the film was examined under transmission electron microscopy (TEM, Hitachi H-7500). For viewing, the film was floated off from the SiO_2 coated silicon wafer onto an HF solution and collected on TEM grids.

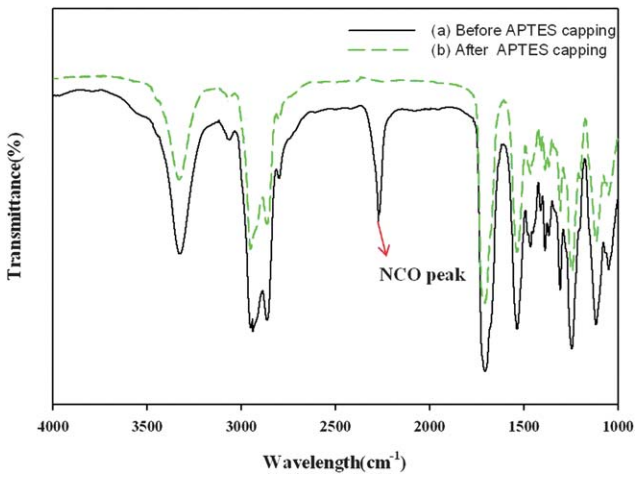

Fig. 1 FT-IR spectra of the PU prepolymer before (a) and after (b) APTES capping.

The shape memory properties were characterized using a UTM that had a heating chamber. For DSME, the sample was first heated to T_g +20 °C and uniaxially stretched to a maximum strain (ε_m) of 100%, followed by cooling and unloading at T_g −20 °C. Upon unloading, a small part of the strain ($\varepsilon_m - \varepsilon_u$) was instantaneously recovered, leaving an unload strain (ε_u). Then, the sample was reheated to T_g +20 °C to recover the strain, leaving a substantial amount of permanent strain (ε_p). These three steps complete one thermomechanical cycle. Shape fixity (R_f) and shape recovery (R_r) ratios for the cycle are defined as:[22]

$$\text{Shape fixity ratio, } R_f = \frac{\varepsilon_u}{\varepsilon_m} \quad (1)$$

$$\text{Shape recovery ratio, } R_r = \frac{\varepsilon_r}{\varepsilon_m} \quad (2)$$

where $\varepsilon_r = \varepsilon_m - \varepsilon_p$ is the recovered strain.

To determine the TSME of the bilayer film, deformation was performed with two steps. First, the film was heated and uniaxially stretched to ε_{mB} at T_{high} where both films are in the rubbery state. Then the film was cooled to T_{mid} where the P35 layer was glassy and the P70 layer was rubbery. Upon releasing the stress, a temporary shape B was fixed with

$$R_{fB} = \varepsilon_{uB}/\varepsilon_{mB} \quad (3)$$

where ε_{mB} and ε_{uB} are the maximum and the unloading strains, respectively. At this temperature, the deformed shape of P35 was frozen. In the second step, the film was further stretched to ε_{mA} at

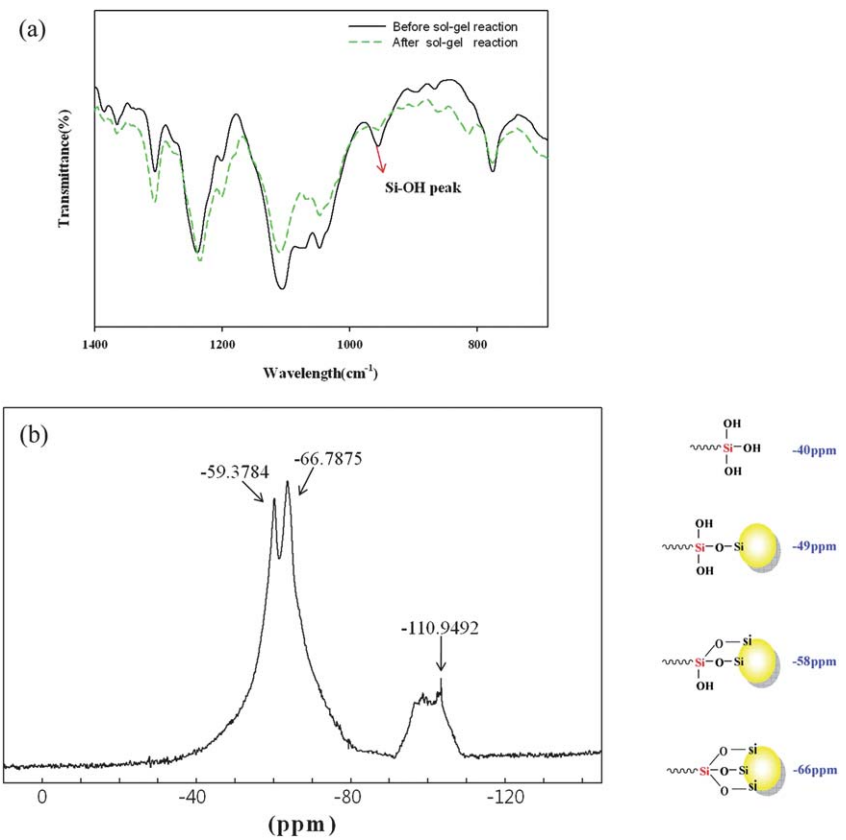

Fig. 2 FT-IR spectra of the silica before and after reaction with APTES (a), and NMR spectrum (b) after reaction with APTES.

T_{mid} and cooled to T_{low} while keeping the strain at ε_{mA}. Upon releasing the stress, a second temporary shape A was fixed as:

$$R_{fA} = [\varepsilon_{uA} - \varepsilon_{uB}]/[\varepsilon_{mA} - \varepsilon_{uB}] \quad (4)$$

where ε_{mA} and ε_{uA} are the maximum and unloading strains, respectively, of this step.

Finally, reheating to T_{high} recovered shapes B and C as:

$$R_{rB} = [\varepsilon_{uA} - \varepsilon_{pB}]/[\varepsilon_{uA} - \varepsilon_{uB}] \quad (5)$$

$$R_{rC} = [\varepsilon_{pB} - \varepsilon_{pC}]/\varepsilon_{uB} \quad (6)$$

The overall shape recovery was obtained as:

$$R_r = [\varepsilon_{uA} - \varepsilon_{pC}]/\varepsilon_{uA} \quad (7)$$

T_{low}, T_{mid}, and T_{high} were respectively set to 10, 45, and 100 °C where $\varepsilon_{mB} = 50$ and $\varepsilon_{mA} = 100\%$. Details are given in Fig. 7.

3. Results and discussion

3.1 Confirmation of APTES capping by FT-IR spectroscopy

The FT-IR spectra of the NCO-terminated PU and APTES capped PU are shown in Fig. 1. The figure shows that the absorption peak at about 2270 cm^{-1} corresponding to the stretch vibration of the NCO group has completely disappeared upon capping with APTES.

3.2 Confirmation of sol–gel reaction by FTIR and Si NMR

The FTIR spectra of the virgin silica and the silica after the reaction with APTES were confirmed in Fig. 2(a). The absorption band at 955 cm^{-1}, assigned to the stretching of the terminal Si–OHs of the silica, almost disappeared after the sol–gel reactions.

The Si NMR spectrum (Fig. 2 (b)) shows three peaks at approximately −58, −66 and − (93–112) ppm. The first two peaks are respectively assigned to P^2 and P^3 species representing silicon atoms with two and three siloxane linkages.[23] The peak at around −(93–112) ppm is for nanosilica (Aerosil 200). There is no evidence of any peaks associated with P^1 (−49 ppm) or P^0 (−40 ppm) species indicating that condensation reactions proceeded almost completely. However, it is mentioned that the APTES monomer has three ethoxy groups it can, in principle, form 100% P^3 species when it is fully condensed.

3.3 TEM images

The TEM images of the nanocomposites are shown in Fig. 3 where the silica particles are well dispersed in the polymer matrix. The average particle dimensions were 12.64 (1%), 30.18 (3%), and 40.72nm (5% silica) with corresponding standard deviations of 2.12, 19.42, and 21.86% respectively. Neither series aggregates nor agglomerates of the silica particles are seen even at the highest particle concentration. The fine dispersion should be important to determine the mechanical properties of the nanocomposites.[14]

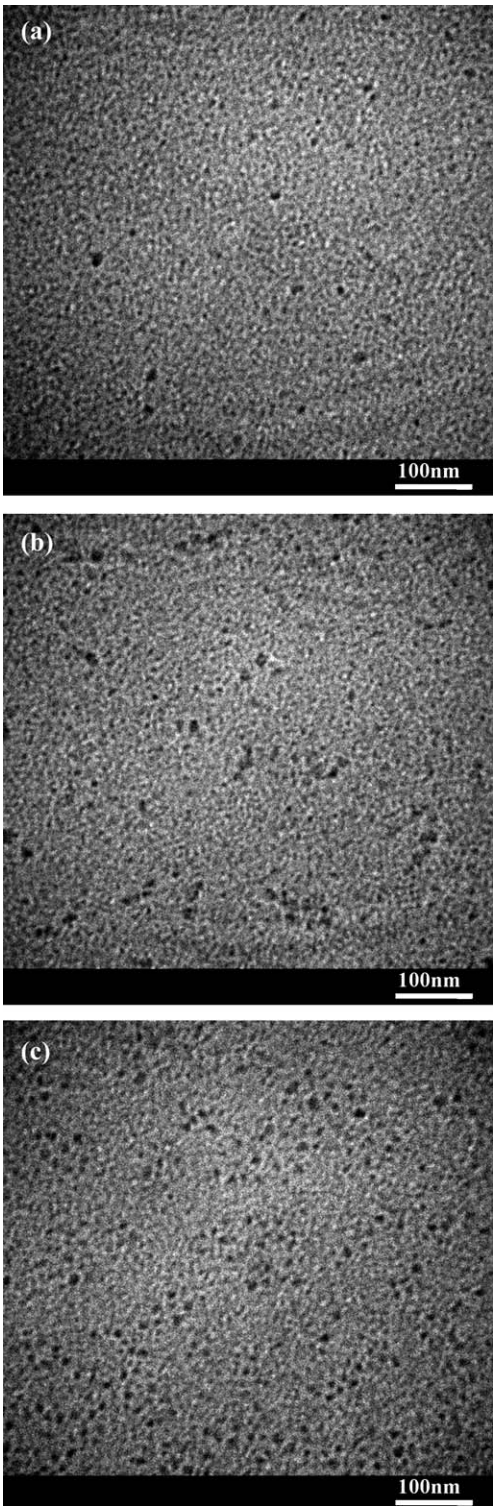

Fig. 3 TEM images of the polyurethane–silica nanocomposite: 1% (a), 3% (b), and 5% silica (c).

3.4 Mechanical properties

The stress–strain behavior of the nanocomposites at 25 °C is shown in Fig. 4. The curves are the average of five measurements, and detailed values including initial modulus, yield and break strengths, and elongation at break are shown in Table 1 with

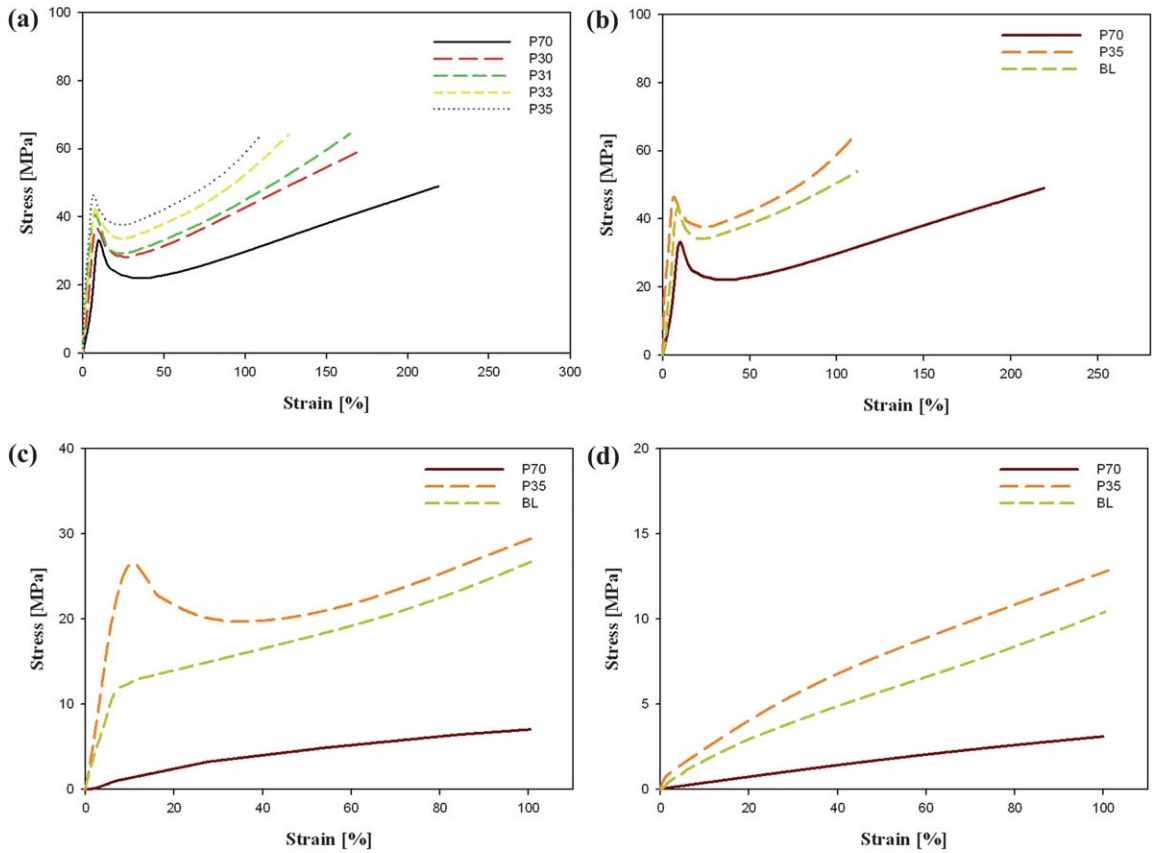

Fig. 4 Stress–strain behaviour of the polyurethane–silica nanocomposites at 25 (a, b), 45 (c), 80 °C (d).

statistical analysis. PU cross-linked by APTES exhibits positive yield, necking, and strain hardening. The initial modulus, yield strength, and break strength are larger for P30 (3000 M_{PU}) than for P70 (7000 M_{PU}) due to the greater cross-link density of P30.

With the addition and increasing amount of silica particles, the modulus, yield strength, and break strength monotonically increase and elongation at break decreases, which is expected from the fine dispersion of silica particles. This led to the increased area under the curve at given elongations. The area is important in SMPs since it is the strain energy stored during stretching, which drives strain recovery upon release of stress in an SMP's rubbery state. The enhanced mechanical properties are based on the dual effects of the silica nanoparticles as multifunctional cross-links and reinforcing fillers. Multifunctional cross-links provide the materials with high cross-link densities while fillers augment the rigidity of the materials.[26] The temperature dependent stress–strain behavior of the bilayer (BL) made of P70 and P35 are shown in Fig. 4 (b)–(d). At 25 °C, all the films show typical glassy behavior. The BL breaks when P35 breaks since the load is already greater than the break strength of P35. At 45 °C, P35 exhibits glassy behavior while P70 exhibits rubbery behavior. Yielding is blunted in the BL due to the continuous increase of stress with P70. At 80 °C all the films exhibit rubbery behavior. It is obvious that most load of the BL is carried by P35 at all temperatures, and the BL carries more load than the simple additive rule (middle of the two curves). The latter should emphasize the importance of interfacial adhesion of the two layers.

3.5 Dynamic mechanical properties

Fig. 5 shows the dynamic mechanical properties of the polyurethane nanocomposites. All the samples show well-defined rubbery plateaus, indicative of cross-linked structures. In addition they show relatively narrow glass to rubber transitions due to the intensive phase mixing of soft and hard segments, and about three orders of magnitude difference in glass and rubbery state moduli. Both properties are highly desirable for shape memory applications.[3] In the design of bilayer TSME materials, the combination of high T_g-high glassy modulus and low T_g-low rubbery modulus materials is important to fix a shape at an intermediate temperature since the glassy material tends to fix its shape while the rubbery material tends to recoil.[21]

The plateau modulus (G_N^o) and tanδ peak temperature increase with the addition and increasing amount of silica particles as well as with decreases of M_{PU}. Silica particles have dual roles: filler and multifunctional cross-link. Filler silica particles augment the rigidity and retard segmental motion of the polymer chains by increasing the T_g.[12] As cross-links, the effect of the silica particles is properly described by the rubber elasticity where the plateau modulus is given by the following equation:[24]

$$G_N^o = \frac{\rho RT}{M_c} = NkT \quad (8)$$

where ρ is the density, T is the absolute temperature, R is the gas constant, and k is the Boltzmann constant. Also, M_c is the molecular weight between the cross-links, and N is the number

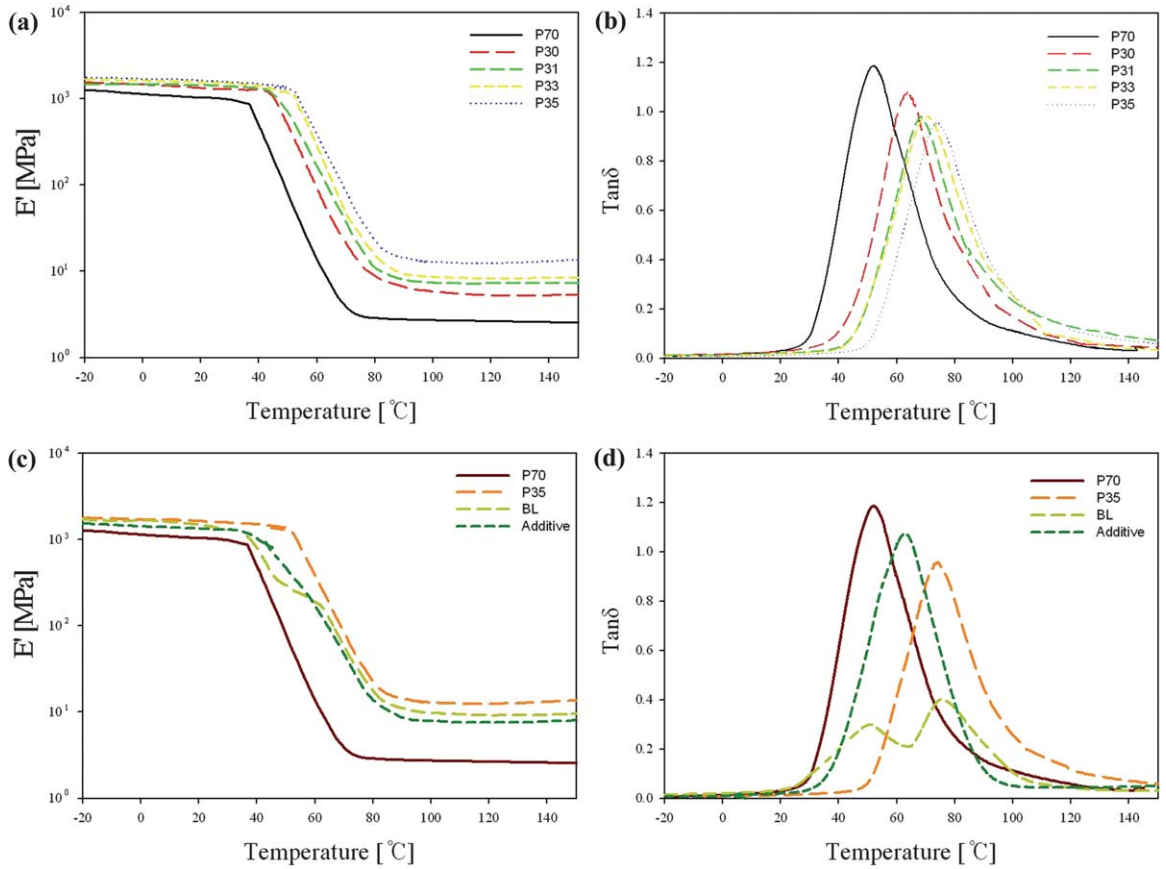

Fig. 5 Storage modulus (a, c) and tanδ (b, d) of the polyurethane–silica nanocomposites *vs.* temperature.

density of the PU subchains that is increasing linearly with the cross-link functionality. It is obvious that the amount of chemically incorporated silica particles and M_{PU} are the key parameters for controlling the elastic properties of the nanocomposites.

The storage modulus of the BL shows an intermediate plateau between 40 and 60 °C and two well-separated tanδ peaks each corresponding to either P70 or P35. The existence of two transitions is due the phase-separated structure of the bilayer film. The rubbery plateau of the BL is greater than that expected by the simple additive rule.

3.6 Shape memory behavior

(A) DSME. The typical cyclic loading and unloading behavior of the PU nanocomposites operating between T_{high} and T_{low} (80 and 10 °C) are shown in Fig. 6 for the first four cycles and the detailed data are given in Table 2. Both types of the unfilled film are in the rubbery state at 80 °C and glassy state at 10 °C. The shape fixity and shape recovery of P30 were 92–96% while those of P70 were 90–95% for the first four cycles. The difference was due to the difference in cross-link density of the two films. For the P30 series, the shape fixity and shape recovery increased to 98–99% with the incorporation of 1% or more silica. More importantly, these properties are mostly retained during the four thermo-mechanical cycles. This resulted in a significant improvement in hysteresis resistance over the unfilled film due to the triple effects of the silica particles as multifunctional cross-linker, reinforcing filler, and stress relaxation retarder.[14] The hysteresis resistance is important since SMPs are often subjected to repeated loading and unloading, such as in footwear and dental applications.[25,26]

When the sample was operated between T_{high} and T_{mid} (80 and 45 °C), P35 exhibited a normal SM behavior (≥95%) while P70 was not fixed (3%) since it was in a rubbery state (Table 3). When the film was operated between T_{mid} and T_{low} (45 and 10 °C), P70 exhibited 90% shape fixity and 96% shape recovery while P35 exhibited 99% fixity but only 2% recovery. At 45 °C, P70 was in the rubbery state while P35 was in the glassy state. The rubbery state seems unnecessary to fix the shape but essential to recover the strain.

(B) TSME. The TSME programming and performance are shown in Fig. 7. An as-fabricated sample was first heated and strained to 50% at 80 °C followed by cooling and stress release at 45 °C. This step yielded an unloading strain (ε_{uB}) of about 40% and shape fixity (R_{fB}) of about 80%. P35 carries about 80% of the stretch load (Fig. 4(d)). For this step, shape fixity depended on the balance between the glassy modulus of P35 and the rubbery modulus of P70 since the former tends to fix and the latter to recoil the sample. At 45 °C, the ratio is approximately four (Fig. 5), which agrees with the shape fixity of about 80%. The combination of a high glassy modulus and low rubbery modulus is desired for this step.

The second step is to stretch the sample from ε_{uB} to m_e (100%) at 45 °C, followed by cooling to 10 °C and the subsequent releasing of the stress. During stretching, P35 carries about 80%

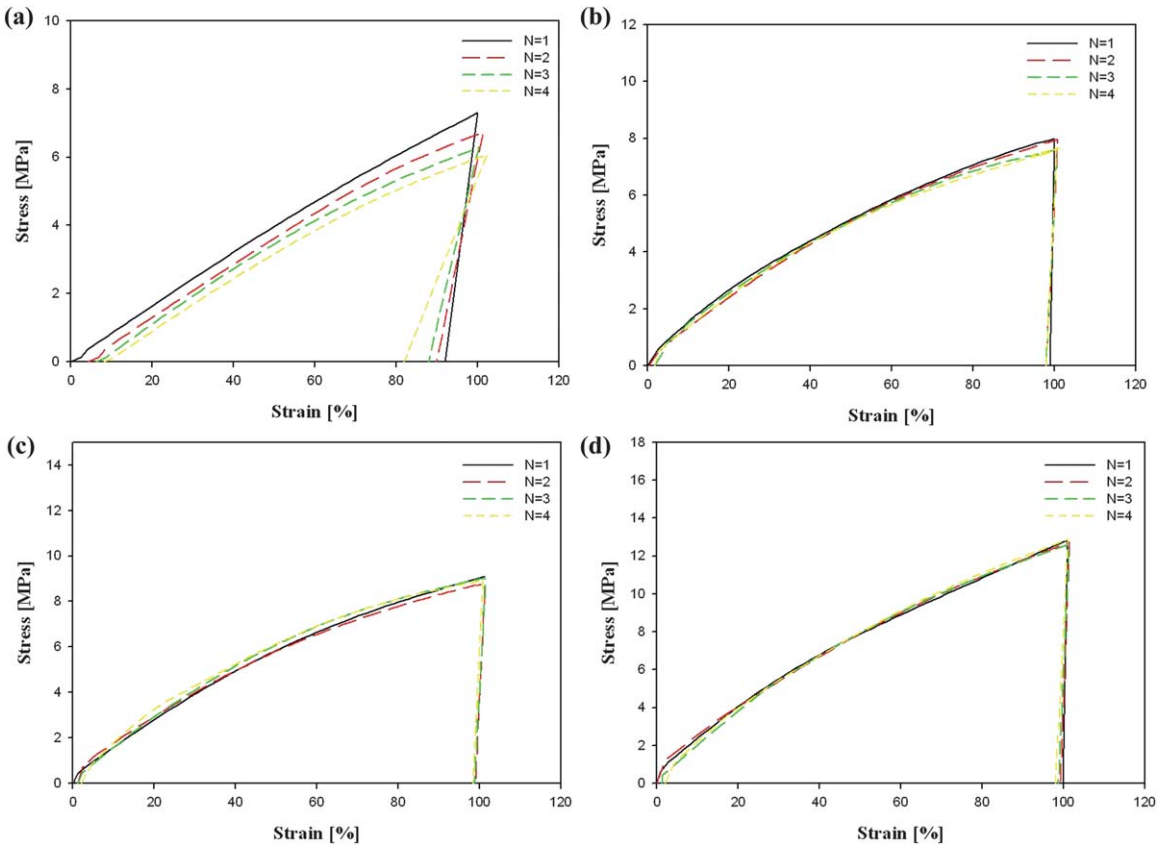

Fig. 6 Thermomechanical cyclic behavior of P30 (a), P31 (b), P33 (c), and P35 (d).

Table 2 Shape fixity and shape recovery of polyurethane–silica nanocomposites (N = number of thermomechanical cycle)

	Shape fixity (%)					Shape recovery (%)				
	P30	P31	P33	P35	P70	P30	P31	P33	P35	P70
N = 1	92	99	99	99	90	96	98	99	99	95
N = 2	90	98	98	99	85	94	98	99	99	94
N = 3	88	98	98	98	84	92	98	98	98	89
N = 4	82	98	98	98	82	89	98	98	98	87

of the load which induces its structural orientation, of which 99% is frozen at 10 °C. The remaining load is carried by P70 and it induces its structural orientation, of which 90% is frozen at 10 °C. This fixing step gave an $R_{fA} \sim 85\%$ which is lower than P35 and P70 operating at 10 and 80 °C. The low stretch temperature, which allows for less orientation relaxation during stretching, seems to be the main reason for the low fixity since the unrelaxed chains tended to recoil.

Table 3 Shape fixity and shape recovery of P70 and P35 after the first four thermomechanical cycles operating at different temperatures

	10–45 °C		45–80 °C		10–80 °C	
	P70	P35	P70	P35	P70	P35
Shape fixity (%)	90	99	3	95	90	99
Shape recovery (%)	96	2	-	97	95	99

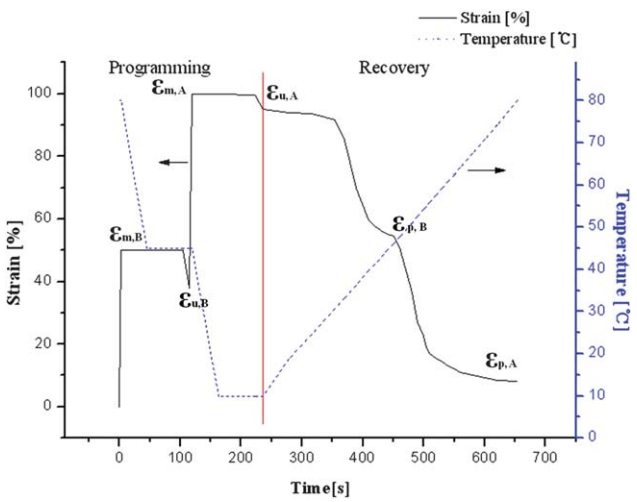

Fig. 7 Triple-shape memory cycles for the bilayer (BL).

As the sample is reheated to T_{high}, about half of the strain is recovered at 45 °C and the other half at 80 °C. Recovery at 45 °C (R_{rB}) is mainly due to P70 while that at 80 °C (R_{rC}) is due to P35. The overall shape recovery (R_r) is about 85% which is lower than P35 and P70 and is mainly due to the lower fixity of the bilayer, which is due to the recoiling tendency of P70 at 45 °C, and low stretch temperature in the second step. The whole process was performed in about 10 min.

4. Conclusions

Shape memory polyurethane–silica nanocomposites have been synthesized by sol–gel reactions between silica particles and polyurethane that was end capped with 3-amino-propyltriethoxysilane. It was shown that the silica particles act as multifunctional cross-links and reinforcing fillers. Consequently, glassy and rubbery modulus, strength, glass transition temperature, and shape memory properties were significantly increased with the addition and increasing content of silica as well as with the decrease in sub-chain molecular weight (M_p).

The bilayer formed from the two independently synthesized films *via* an interpenetrating polymer network that exhibited synergistic properties in terms of modulus and strengths due to the cohesive adhesion of the two layers. In addition, the bilayer exhibited two undisturbed T_gs by which an intermediate plateau region and a TSME that exhibited a sufficiently high SM performance were defined. It is concluded that the TSME can be easily tailored by two or more independent films with different T_gs and a high glass/low rubbery modulus ratio.

5. References

1 S. Madbouly and A. Lendlein, *Adv. Polym. Sci.*, 2010, **226**, 41–95.
2 B. K. Kim, *eXPRESS Polym. Lett.*, 2010, **4**, 589.
3 C. Liu, H. Qin and P. T. Mather, *J. Mater. Chem.*, 2007, **17**, 1543–1558.
4 D. Ratna and J. Karger-Kocsis, *J. Mater. Sci.*, 2008, **43**, 254–269.
5 H. Meng and J. Hu, *J. Intell. Mater. Syst. Struct.*, 2010, **21**, 859–885.
6 W. Small IV; P. Singhal T. S. Wilson; D. J. Maitland 2009, Lawrence Livermore National Lab-JRNL-412712.
7 U. NarendraKumar, K. Kratz, W. Wagermaier, M. Behl and A. Lendlein, *J. Mater. Chem.*, 2010, **20**, 3404–3415.
8 P. T. Knight, K. M. Lee, H. Qin and P. T. Mather, *Biomacromolecules*, 2008, **9**, 2458–2467.
9 F. Cao and S. C. Jana, *Polymer*, 2007, **48**, 3790–3800.
10 C. Liang, C. A. Rogres and E. J. Malafeew, *J. Intell. Mater. Syst. Struct.*, 2007, **8**, 380–386.
11 T. Ohki, Q. Ni, N. Ohako and M. Iwamoto, *Composites, Part A*, 2004, **35**, 1065–1073.
12 M. K. Jang, A. Hartwig and B. K. Kim, *J. Mater. Chem.*, 2009, **19**, 1166–1172.
13 D. H. Jung, H. M. Jeong and B. K. Kim, *J. Mater. Chem.*, 2010, **20**, 3458–3466.
14 T. Pretsch, *Smart Mater. Struct.*, 2010, **19**, 015006.
15 M. Behl and A. Lendlein, *J. Mater. Chem.*, 2010, **20**, 3335–3345.
16 I. Bellin, S. Kelch, R. Langer and A. Lendlein, *Proc. Natl. Acad. Sci. U. S. A.*, 2006, **103**, 18043–18047.
17 S. J. Chen, J. L. Hu and H. T. Zhuo, *Compos. Sci. Technol.*, 2010, **70**, 1437–1443.
18 S. J. Hong, W. R. Yu and J. H. Youk, *Smart Mater. Struct.*, 2010, **19**, 035022–9.
19 Z. D. Wang, Z. F. Li and L. Y. Wang, *J. Appl. Polym. Sci.*, 2010, **118**, 1406–1413.
20 I. M. Pereira and R. L. Orefice, *Polymer*, 2010, **51**, 1744–1751.
21 T. Xie, X. C. Xiao and Y. T. Cheng, *Macromol. Rapid Commun.*, 2009, **30**, 1823–1827.
22 B. K. Kim, S. Y. Lee and M. Xu, *Polymer*, 1996, **37**, 5781–5793.
23 S. M. De Paul, J. W. Zwanziger, R. Urich, W. Wiesner and H. W. J. Spiess, *J. Am. Chem. Soc.*, 1999, **121**, 5727–5736.
24 U. W. Gedde; "*Polymer Physics*", Klumer Academic Publishers, London, 1999.
25 J. H. Yang, B. C. Chun, Y. C. Chung and J. H. Cho, *Polymer*, 2003, **44**(11), 3251–3258.
26 I. S. Kolesov and H.-J. Radusch, *eXPRESS Polym. Lett.*, 2008, **2**(7), 461–473.